Nanoscale Advances

ROYAL SOCIETY OF CHEMISTRY

PAPER

View Article Online
View Journal | View Issue

Cite this: *Nanoscale Adv.*, 2024, **6**, 973

Cocktail of lipophilic and hydrophilic chemotherapeutics in high-load core@shell nanocarriers to treat pancreatic tumours

David Rudolph,[a] Myrto Ischyropoulou,[bc] Juliana Pfeifer,[d] Joanna Napp, *[bc] Ute Schepers, *[d] Frauke Alves *[bce] and Claus Feldmann *[a]

ITC/Toc@$Gd_2(FLP)_3$ core@shell nanocarriers with a chemotherapeutic cocktail of lipophilic irinotecan (ITC) as the particle core and hydrophilic fludarabine phosphate (FLP) in the particle shell are realized. They are prepared *via* a microemulsion approach with ITC dissolved in tocopherol (Toc) as droplet phase and stabilized by water-insoluble $Gd_2(FLP)_3$. The synthesis can be followed by zeta-potential analysis. X-ray powder diffraction, infrared spectroscopy, elemental analysis, thermogravimetry, and photometry show a drug load of 49 μg per mL ITC and 317 μg per mL FLP at a nanocarrier concentration of 1.5 mg mL^{-1}. Size and structure are evidenced by electron microscopy, resulting in a total diameter of 45 ± 16 nm, an inner core of 40 ± 17 nm, and a shell of 3–8 nm. *In vitro* studies with different cancer cell lines (*i.e.*, human melanoma/SK-Mel-28, cervical cancer/HeLa, mouse pancreatic cancer/Panc02 and KPC as well as human pancreatic cancer/Capan-1 cells) prove efficient nanocarrier uptake and promising cytostatic efficacy. Specifically for KPC cells, ITC/Toc@$Gd_2(FLP)_3$ nanocarriers show an increased efficacy, with half maximal inhibitory concentration (IC_{50}: 4.2 μM) > 10 times lower than the free drugs (IC_{50}: ITC: 47.7 μM, FLP: 143 μM). This points to the synergistic effect of the ITC/FLP drug cocktail in the nanocarriers and may result in a promising strategy to treat pancreatic ductal adenocarcinoma (PDAC).

Received 1st September 2023
Accepted 24th December 2023

DOI: 10.1039/d3na00720k

rsc.li/nanoscale-advances

Introduction

Oncology belongs to the very first areas of application, for which drug-loaded nanocarriers received clinical approval.[1] Here, non-PEGylated liposomal doxorubicin (Myocet®) or PEGylated liposomal doxorubicin (CAELYX®, DOXIL®) are typical examples.[2] Such nanocarrier formulations are expected to have specific advantages over the freely dissolved chemotherapeutics, including an increased drug accumulation in the tumour, the use of higher doses over shorter periods of time, less side effects, and/or a reduced off-target uptake.[1,2a] In difference to freely dissolved drugs, nanocarriers also offer the option of straightforward tracking for instantaneous assessment of drug delivery and targeting.[3]

Current nanocarrier concepts often suffer from inadequate drug loading (often <20% of total nanocarrier mass), high material complexity, uncontrolled drug leakage, limited cell uptake, damage of cell membranes, unexpected toxicity and/or hypersensitivity.[4] Typically, the active drug is encapsulated in certain matrix material such as organic polymers (*e.g.* polyethyleneglycol/PEG) or biopolymers (*e.g.*, polysaccharides, polypeptides),[5] liposomes or micelles,[6] or inorganic matrices such as silica, iron oxides, and metal phosphates.[7] Here, the matrix material usually represents the majority phase of the nanocarrier (often >80% of total nanocarrier mass) and – although not being an active drug – the matrix material may nevertheless cause toxic or allergic effects and needs to be biodegradable to ensure a complete release from the body. Moreover, current nanocarrier formulations predominately contain only a single drug. Nanocarriers with a combination of several cytostatic agents were yet barely addressed although state-of-the-art clinical tumour therapy relays on drug cocktails with two or more chemotherapeutics (*e.g.* FOLFIRINOX® with 5-fluorouracil, irinotecan and oxaliplatinum).[7] Drug cocktails with two or more chemotherapeutics and different pharmacological properties for a simultaneous release at the site of the tumour with high concentration are highly desirable to reduce the therapeutic dose, to enhance the anticancer efficacy due to synergistic effects, and/or to minimize the risk of multi-drug

[a]*Institute for Inorganic Chemistry (IAC), Karlsruhe Institute of Technology (KIT), Engesserstraße 15, 76131 Karlsruhe, Germany. E-mail: claus.feldmann@kit.edu*
[b]*University Medical Center Goettingen (UMG), Institute for Diagnostic and Interventional Radiology, Robert-Koch-Straße 40, 37075 Göttingen, Germany. E-mail: falves@gwdg.de; joanna.napp@med.uni-goettingen.de*
[c]*Max-Planck-Institute for Multidisciplinary Sciences (MPI-NAT), Translational Molecular Imaging, Hermann-Rein-Straße 3, 37075, Göttingen, Germany*
[d]*Institute of Functional Interfaces, Karlsruhe Institute of Technology (KIT), Hermann-von-Helmholtz-Platz 1, 76344 Eggenstein-Leopoldshafen, Germany. E-mail: ute.schepers@kit.edu*
[e]*Clinic of Hematology and Medical Oncology, University Medical Center Göttingen, Robert-Koch-Straße 40, 37075 Göttingen, Germany*

resistance.[8] To this regard, nanocarrier-based platforms can be highly promising.[9]

Aiming at novel chemotherapeutic nanocarriers, we here specifically aim at drug cocktails and achieving a high drug load of the nanocarriers (>50% of total nanocarrier mass).[10] As a proof-of-the-concept, we have selected two chemotherapeutics with different properties: fludarabine phosphate (FLP) and irinotecan (ITC). FLP is highly hydrophilic, water soluble and blocks the enzymes ribonucleotide reductase and DNA polymerase, which are important for cell division and DNA synthesis.[11] ITC inhibits topoisomerase I and is – in contrast to FLP – lipophilic and poorly soluble in water.[12] Accordingly, FLP and ITC exhibit different mechanisms of action and are both known for high activity not only against pancreatic ductal adenocarcinoma (PDAC), but also against other solid tumors and blood cancers in both clinical and experimental settings.[13] Especially for PDAC, which is the most common type of pancreatic cancer (90% of incidences) with a 5 years survival rate of only 8%,[14] due to late detection, tumor heterogeneity, intrinsic chemoresistance and treatment failure.[15] Thus, there is an urgent need for novel therapeutic strategies and novel multidrug delivery systems, which hold the promise to prolong survival and quality-of-life for chemotherapy-treated PDAC patients.

Experimental section

Nanocarrier synthesis

Chemicals. Sodium dodecylsulfate (SDS, ≥99.0%, Sigma-Aldrich, Germany), *n*-butanol (>99.5%, Riedel-de-Haën, Germany), α-tocopherol (97%, ABCR, Germany), trisodium citrate (99%, Carl Roth, Germany), gadolinium chloride hexahydrate (>99%, Sigma-Aldrich), irinotecan (98%, ABCR, Germany), sodium adenosine monophosphate (>99%, Sigma-Aldrich, Germany), DUT549P1-aadUTP (Dyomics, Germany), ATTO647N-aadUTP (≥95%, Jena Bioscience, Germany) and fludarabine phosphate (>99%, Sigma-Aldrich, Germany) were used as purchased.

Formation of microemulsion. An oil-in-water microemulsion (o/w-ME) was established by mixing 2.5 mL (140 mmol) of demineralized water, 0.4 mL (0.38 g, 0.88 mmol) of tocopherol (Toc) as the lipophilic droplet phase, 700 mg (2.43 mmol) of sodium dodecylsulfate (SDS) as the surfactant, and 0.45 mL (0.36 g, 4.91 mmol) of *n*-butanol as the co-surfactant. After mixing, a yellowish, transparent, and colloidally stable microemulsion was obtained at room temperature.

Synthesis of ITC/Toc@$Gd_2(FLP)_3$ nanocarriers. 3.7 mg of ITC (6.31 μmol) were dissolved in 0.5 mL of the aforementioned microemulsion and diluted with 10 mL of demineralized water. 2.1 mL of the microemulsion were added over a period of 1 min to a solution of 25 mg of $GdCl_3 \cdot 6H_2O$ (67.3 μmol) and 20 mg of NH_4Ac (259 μmol) in 10 mL of demineralized water and stirred for 10 min. The resulting suspension was centrifuged (10 000 × *g*, 5 min). Thereafter, the centrifugate was resuspended in 10 mL of ammonium acetate solution (20 mg, 259 μmol) by ultrasonic irradiation (Bandelin Sonoplus HD 2070, Germany) with an amplitude of 50% for 3 min. Upon further ultrasonic treatment (1 min), a solution of H_2(FLP) (10 mg, 27.4 μmol) was added over a period of 10 s.

For fluorescence labelling of the nanocarriers, 50 μL of a solution with the nucleotide-based dyes Dyomics DUT 549-aadUTP or ATTO 647-aadUTP (50 nmol) was added to the H_2(FLP) solution prior to injection. Finally, the suspension was adjusted to pH 8 by addition of 0.1 M NaOH and stirred for additional 10 min. After centrifugation (20 000 × *g*, 10 min), the fluorescence-labelled nanocarriers were centrifuged/redispersed from/in demineralized water. Finally, they were resuspended in sodium citrate solution (18.6 μmol) or dried in vacuum at room temperature to obtain powder samples.

The synthesis of Toc@$Gd_2(AMP)_3$ nanoparticles (AMP: adenosinemonophosphate) as drug-free negative control followed the same synthesis procedure. It must be noticed that no ITC was dissolved in the microemulsion. Moreover, a solution of Na_2(AMP) (9.5 mg; 27.4 μmol) in 5 mL of water was added instead of a solution of H_2(FLP).

Analytical equipment

Scanning electron microscopy (SEM). SEM was carried out with a Zeiss Supra 40 VP microscope (Zeiss, Germany), equipped with a Schottky field emitter (2.0 nm resolution). To this concern, diluted aqueous suspensions of the ITC/Toc@$Gd_2(FLP)_3$ nanocarriers were deposited on silicon wafers and left for drying overnight. The acceleration voltage was in the range of 5–20 kV; the working distance was 2–3 mm. Average particle diameters were calculated by statistical evaluation of at least 150 nanoparticles (ImageJ 1.47v software).

Transmission electron microscopy (TEM). TEM and high-angle annular dark-field scanning transmission electron microscopy (HAADF-STEM) were conducted with a FEI Osiris microscope at 200 kV (FEI, The Netherlands). TEM samples were prepared by evaporating aqueous suspensions of the ITC/Toc@$Gd_2(FLP)_3$ nanocarriers on amorphous carbon (Lacey)film suspended on copper grids. Average particle diameters were calculated by statistical evaluation of at least 150 nanoparticles (ImageJ 1.47v software).

Energy-dispersive X-ray (EDX) spectroscopy. High-resolution EDXS was performed to analyse the chemical composition of single ITC/Toc@$Gd_2(FLP)_3$ nanocarriers. The spectra were obtained at 200 kV electron energy with a FEI Osiris microscope equipped with a Bruker Quantax system (XFlash Detector, Bruker, Germany). EDX spectra were quantified with the FEI software package "TEM imaging and analysis" (TIA). Using TIA, element concentrations were calculated on the basis of a refined Kramers' law model that includes corrections for detector absorption and background subtraction. Standardless quantification, *i.e.* by means of theoretical sensitivity factors, without thickness correction was applied. EDX spectra were taken in the STEM mode with a probe diameter of 0.5 nm. Using a focused electron probe, EDXS area scans were performed to obtain average compositions of larger sample regions. EDX spectra were acquired by continuously scanning the probe in the predefined region.

Dynamic light scattering (DLS). DLS was used to determine the hydrodynamic diameter of the as-prepared ITC/Toc@$Gd_2(FLP)_3$ nanocarriers in aqueous suspension. Studies were

conducted at room temperature in polystyrene cuvettes applying a Nanosizer ZS (Malvern Instruments, United Kingdom).

X-ray powder diffraction (XRD). X-ray powder diffraction (XRD) was performed with a Stoe STADI-MP diffractometer (Stoe, Germany) operating with Ge-monochromatized Cu-Kα radiation (λ = 1.54178 Å) and Debye–Scherrer geometry. The dried ITC/Toc@$Gd_2(FLP)_3$ nanocarriers were fixed between Scotch tape and acetate paper and measured between −69° and +69° of two-theta.

Fourier-transformed infrared spectroscopy (FT-IR). FT-IR spectra were recorded on a Bruker Vertex 70 FT-IR spectrometer (Bruker, Germany). All ITC/Toc@$Gd_2(FLP)_3$ nanocarrier samples and references were pestled and diluted with KBr (3 mg of sample per 300 mg of KBr) and pressed to pellets.

Elemental analysis (C/H/N/S analysis). C/H/N/S analysis was performed *via* thermal combustion with an Elementar Vario Microcube device (Elementar, Germany) at a temperature of about 1100 °C.

Optical spectroscopy (UV-vis). UV-vis spectroscopy was used to quantify the amount of ITC and FLP in the respective ITC/Toc@$Gd_2(FLP)_3$ nanocarriers according to the Lambert–Beer formalism.[16] The respective concentrations were quantified in comparison to reference solutions with known concentrations by applying calibration curves. UV-vis spectra were recorded with an UV2700 from Shimadzu (Japan). Nanoparticle suspensions were measured in polystyrene cuvettes in an integrating sphere in diffuse transmission geometry against the corresponding pure solvent as a reference.

Fluorescence spectroscopy (FL). FL was examined with a Horiba Jobin Yvon Spex Fluorolog 3 (Horiba Jobin Yvon, France) equipped with a 450 W Xe lamp. Nanocarrier suspensions were measured in polystyrene cuvettes.

Cell studies

Cell culture. MH-S murine alveolar macrophage cell line, Panc02 [17] and KPC murine PDAC cell lines[18,19] as well as Capan-1 human cell line[20] were used.

MH-S cells were bought from ATCC (CRL-2019™)[21] and Panc02 cells were kindly provided by Dr S. F. Pedersen (Section for Cell Biology and Physiology, Department of Biology, Faculty of Science, University of Copenhagen, Denmark). KPC cells (KPCbl6, clone 2.2) were kindly provided by Prof. Dr Volker Ellenrieder (Clinic for Gastroenterology, Gastrointestinal Oncology and Endocrinology, University Medical Center Göttingen, Germany). Capan-1 was bought from ATCC (HTB-79™).

MH-S cells were grown in RPMI medium supplemented with 10% fetal bovine serum (FBS, PAA Laboratories Gold), 0.1% mercaptoethanol, sodium pyruvate, L-glutamine, and D-glucose (Gibco), Panc02 were grown in Dulbecco's Modified Eagle Medium (DMEM, Thermo Fisher Scientific) supplemented with 10% fetal bovine serum (FBS), sodium pyruvate, L-glutamine, and D-glucose (Gibco), KPC in 10% fetal bovine serum (FBS), 1% NEAA (non-essential amino acids), sodium pyruvate, L-glutamine, and D-glucose (Gibco) and Capan-1 in Iscove's Modified Dulbecco's Medium (IMDM) with 20% FBS sodium pyruvate, L-glutamine, and D-glucose (Gibco).

The cell line SK-Mel-28 is a cell line isolated from the skin of male patients with malignant melanoma. The HeLa cell line is the oldest human cell line derived from cervical cancer cells. Both types of cells were cultured in (DMEM, Thermo Fisher Scientific) supplemented with 10% (FBS, Thermo Fisher Scientific) and 1% penicillin/streptomycin (P/S, Thermo Fisher Scientific). All cells were cultivated at 37 °C under a humidified atmosphere of 5% CO_2.

Cytotoxicity and antitumor activity. To study anti-tumor efficacy of the nanoparticles, Panc02 or KPC cells were plated in a 96-well plate at a concentration of 15 000 cells per cm^2 and allowed to attach for 4 h. After, the cells were treated with gradient concentrations according to the FLP content in the IOH-NPs, 10–100 μM of ITC/Toc@$Gd_2(FLP)_3$ and the corresponding amounts of reference IOH-NPs as well as control solutions with ITC, FLP, and the combination of both ITC and FLP. Cell confluence was measured over two weeks, using the live cell imaging system (Incucyte® ZOOM; Sartorius). Phase-contrast images (two images per well) were acquired every hour using a 10× objective. The concentration-dependent efficacy and the half-maximal inhibitory concentration (IC_{50}) were calculated using GraphPad Prism 9 software, based on the cell confluence at 72 h.

MTT assay. For cytotoxicity studies in HeLa and SK-Mel-28 cells, 1×10^4 cells per well were seeded in a 96-well plate and cultured for 24 h. Then, the cells were treated for 1 day with increasing concentrations (10–200 μM) of ITC/Toc@$Gd_2(FLP)_3$ nanocarriers. Afterwards, 3(4,5-dimethylthiazol-2-yl)-2,5-diphenyltetrazolium bromide reagent (MTT, Promega, Germany) was added and after incubation for 3 h, the cells were lysed using 100 μL of MTT solubilization solution (Promega, Germany). The absorbance was measured at a wavelength of 570 nm using a microplate reader (SpectraMax® iD3, Molecular Devices). The experiments were performed in triplicate, and the SD was determined using Student's *t*-test.

Cellular uptake studies. To study the nanocarrier uptake, MH-S, Panc02, KPC and Capan-1 cells with 13 000 cells per cm^2 were plated on coverslips and incubated for different times (30 min, 5, 24, 48 h) with 12.5 ng mL^{-1} of the respective nanocarriers. The coverslips were washed twice with phosphate-buffered saline (PBS), fixed with 4% paraformaldehyde (PFA) for 10 min at room temperature and counterstained and mounted with 4′,6-diamidino-2-phenylindole (DAPI, 1 : 1000, Thermo Fisher Scientific, Germany). Fluorescence was visualized with a SP5 Leica TCS X confocal microscope (Leica Microsystems, Germany).

For the analysis of HeLa and SKMel28 cells, the cells were seeded at the density of 2×10^4 cells per well in an 8-well μSlide from IBIDI plate and cultured for 24 h. Afterwards, the cells were incubated for 1 day with the 50 μg per mL ITC/Toc@$Gd_2(FLP)_3$ nanocarriers, then stained for mitochondria (125 nM MitoTracker™ Green FM, Thermo Fisher Scientific, Germany) and nuclei (2 μg per mL Hoechst 33342, Thermo Fisher Scientific, Germany), and finally examined with fluorescence confocal microscope (STELLARIS 5, Leica Microsystems, Germany).

Microscopy and image analysis. A Leica SP5 TCS X or a Leica STELLARIS 5 confocal laser scanning microscope was used for

fluorescence imaging. For the uptake studies with the MH-S, Panc02, KPC and Capan-1 cells with the respective nanocarriers, the following excitation/emission wavelengths were used/detected: nuclei/DAPI staining (λ_{ex} = 405 nm, λ_{em} = 415–479 nm) and for the nanocarriers (λ_{ex} = 635 nm, λ_{em} = 657–750 nm). For the live imaging of HeLa and SKMel28 cells, the following excitation/emission wavelength were used/detected: nuclei (λ_{ex} = 405 nm, λ_{em} = 410–510 nm), mitochondria (λ_{ex} = 488 nm, λ_{em} = 490–550 nm) and for the nanocarriers (λ_{ex} = 635 nm, λ_{em} = 650–750 nm). Images were analysed with ImageJ.[22]

Statistical analysis. Statistical analysis was performed with GraphPad Prism 9 Software. Significant differences of the mean values between two groups were analysed by *t*-test, with a *p*-value of 0.1 as the margin for statistical significance. All diagrams show mean values ± SEM.

Results and discussion

Synthesis of ITC/Toc@$Gd_2(FLP)_3$ core@shell nanocarriers

ITC/Toc@$Gd_2(FLP)_3$ nanocarriers with a cocktail of lipophilic ITC and hydrophilic FLP were synthesized *via* a microemulsion approach (Fig. 1). First of all, an oil-in-water microemulsion (o/w-ME) was prepared using α-tocopherol as the oil phase, ITC as a lipophilic chemotherapeutic agent as well as sodium dodecylsulfate (SDS) with dodecylsulfate (ds) serving as surfactant and *n*-butanol as co-surfactant (SDS : *n*-butanol = 1 : 2) (Fig. 1a). α-Tocopherol – also known as vitamin E – has the advantage to be highly biocompatible.[23] After mixing and equilibration, a transparent pale yellow microemulsion was obtained with the yellow colour indicating the presence of ITC (Fig. 1c).

In order to stabilize the ITC-containing micellar droplet with a solid shell and in order to add FLP as the second chemotherapeutic agent, an aqueous solution of $GdCl_3 \times 6H_2O$ was added slowly. Gd^{3+} efficiently coordinates to the sulphate groups of ds. On the one hand, this can be directly visualized since changing the surface charge from the negative sulfonate groups of the surfactant to positively charged Gd^{3+} on the surface of the micelles results in a destabilization of the micelle, which causes a colourless fluffy precipitate (Fig. 1d). Moreover, the change of the surface charge can be followed by a zeta-potential analysis (Fig. 1b). Thus, the ITC-containing microemulsion exhibits a highly negative charge of −80 to −100 mV at pH 5–13, which relates to the anionic head groups of ds as the surfactant. After addition of Gd^{3+}, the surface charge decreases to −20 to −50 mV along with the coordination of Gd^{3+} to the sulfate head groups of ds. The reduced surface charge and the cation-based surface termination are causative for the low colloidal stability of the suspension at this point of the synthesis.

As a next step, an aqueous solution of $H_2(FLP)$ was added within about 10 seconds to initiate the formation of a $Gd_2(FLP)_3$ shell around the ITC-filled micellar droplet (Fig. 1a). During the addition, the suspension was homogenized by sonification in order to prevent agglomeration and to ensure the formation of a uniform shell. Upon formation of a $Gd_2(FLP)_3$ shell, the surface charge returns to more negative values of −40 to −65 mV due to coordination of Gd^{3+} with the FLP phosphate groups and the surface termination with the highly polar FLP (Fig. 1b). Again, the course of the synthesis can be also followed with the naked eye since suspensions of the final ITC/Toc@$Gd_2(FLP)_3$ core@shell nanoparticles are colloidally highly stable due to negative surface charging (Fig. 1e). After purification by centrifugation and redispersion to remove dissolved salts and excess starting materials, aqueous ITC/Toc@$Gd_2(FLP)_3$ core@shell nanocarrier suspensions are colloidally stable and do not show precipitation over a period of several weeks.

To allow a fluorescence detection of the ITC/Toc@$Gd_2(FLP)_3$ core@shell nanocarriers, small amounts of nucleotide-based dyes such as Dyomics DUT549P1-aadUTP or ATTO647N-aadUTP can be added together with FLP (Fig. 1). As both dyes contain triphosphate groups, they are encapsulated together with FLP in the nanocarrier shell (Fig. 2a). Successful incorporation of the dyes is confirmed qualitatively by the resulting blue (DUT 549) or pink (ATTO) colour of the nanocarrier

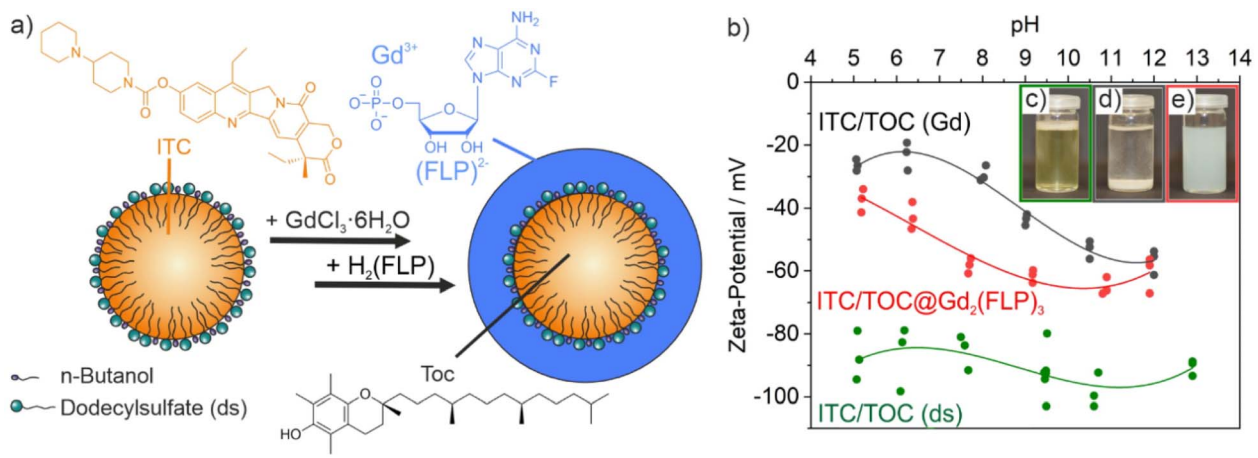

Fig. 1 Synthesis of ITC/Toc@$Gd_2(FLP)_3$ nanocarriers: (a) scheme illustrating synthesis conditions and nanocarrier structure; (b) pH-dependent zeta potential over the course of the synthesis with photos of microemulsion with ds-stabilized ITC/Toc (c), colloidally unstable suspension after addition of Gd^{3+} (d), final suspension of ITC/Toc@$Gd_2(FLP)_3$ core@shell nanocarriers (e).

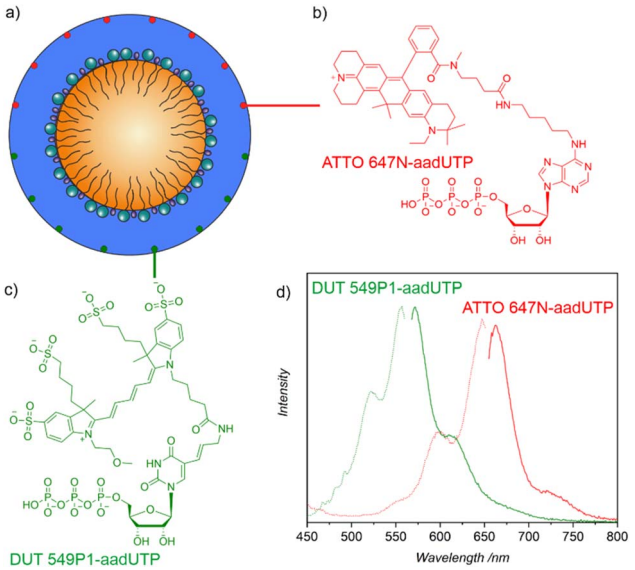

Fig. 2 Fluorescence of ITC/Toc@Gd_2FLP_3 nanocarriers: (a) scheme of core@shell structure with ATTO647N-aadUTP (b) and DUT549P1-aadUTP (c) in the nanocarrier shell, (d) excitation and emission spectra of the labelled nanocarriers with green (DUT549P1-aadUTP: λ_{exc} = 556 nm, λ_{em} = 572 nm) or red (ATTO647N-aadUTP: λ_{exc} = 647 nm, λ_{em} = 664 nm) emission.

suspensions. The presence of the dyes is validated by fluorescence spectroscopy (Fig. 2d). Thus, the nanocarrier suspensions show strong absorption at 450–550 nm (DUT 549) and 525–650 nm (ATTO 647). Green and red emission is observed at 565–725 nm (DUT 549) and 655–775 nm (ATTO 647) with maximum emission at 572 nm for DUT549P1-aadUTP-labelled nanocarriers and maximum emission at 664 nm for ATTO647N-aadUTP-labelled nanocarriers.

Chemical composition of ITC/Toc@$Gd_2(FLP)_3$ nanocarriers

The chemical composition of the as-prepared ITC/Toc@$Gd_2(FLP)_3$ nanocarriers was examined by different methods, including X-ray powder diffraction (XRD), Fourier-transformed infrared (FT-IR) spectroscopy, thermogravimetry (TG), elemental analysis (EA), and photometry (Fig. 3 and 4). According to XRD, the nanocarriers are amorphous, which is to be expected for such organophosphates with voluminous anions and a synthesis at room temperature (Fig. 3c). Aiming at drug release, however, amorphous drug nanocarriers are considered to be advantageous as the dissolution rate is often enhanced in comparison to crystalline drug nanocarriers.[24]

FT-IR spectroscopy, first of all, confirms the presence of phosphate-related vibrations with high intensity (ν(P=O): 1250, 1020 cm^{-1}) and the characteristic carbon–nitrogen stretching

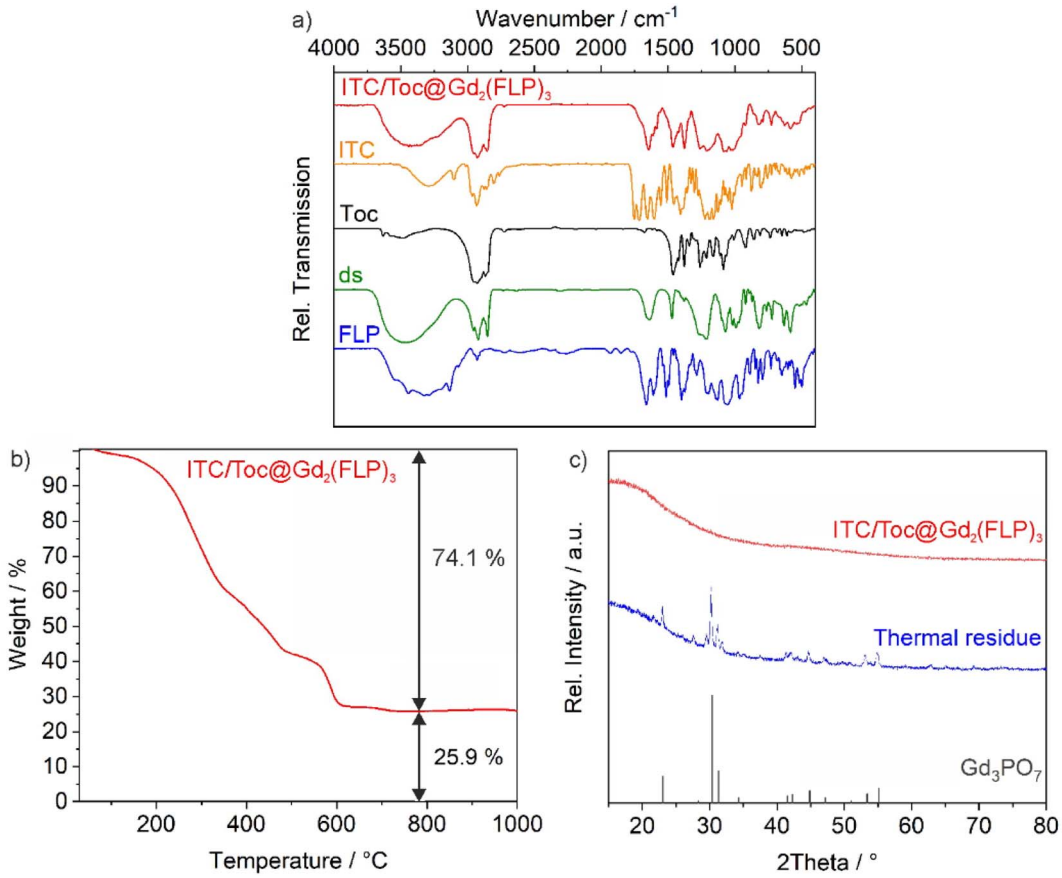

Fig. 3 Chemical composition of the ITC/Toc@$Gd_2(FLP)_3$ nanocarriers: (a) FT-IR spectra with ITC, Toc, SDS and FLP as references; (b) TG analysis; (c) XRD of the as-prepared nanocarriers and of the thermal residue after TG analysis (Gd_3PO_7: ICDD-no. 00-034-1066 as a reference).

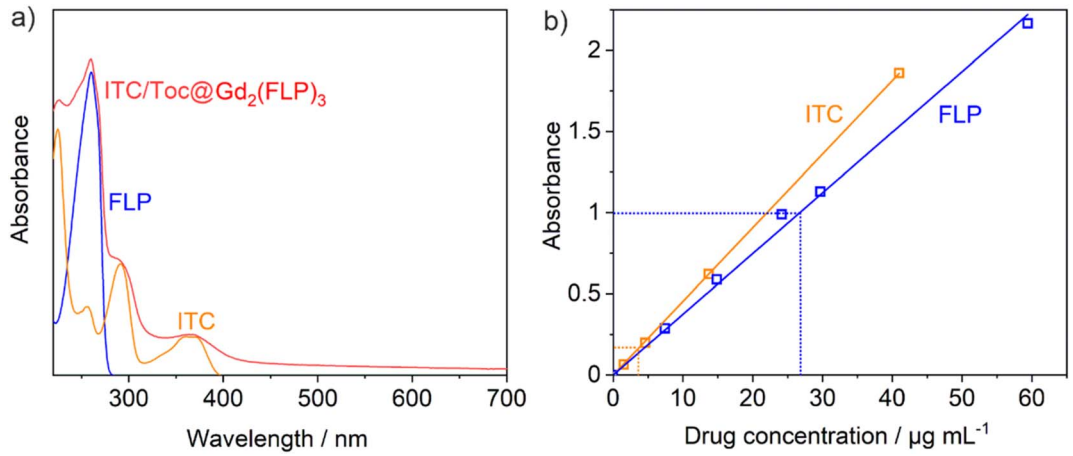

Fig. 4 Photometry of ITC/Toc@$Gd_2(FLP)_3$ nanocarriers: (a) UV-vis spectra of ITC/Toc@$Gd_2(FLP)_3$ suspension with aqueous solutions of ITC (dissolved in a microemulsion with ds as surfactant) and FLP (in water) as references; (b) UV-vis calibration curves for ITC and FLP (nanocarrier sample diluted by a factor of 12 to fit on the calibration curve).

vibrations of the purine ring (ν(C=N): 1610 cm^{-1}) that are both related to FLP. Furthermore, the presence of Toc and ds is confirmed by carbon–hydrogen stretching vibrations of the alkyl chains (ν(C–H): 3000–2850 cm^{-1}) and the characteristic sulfur–oxygen stretching vibrations (ν(S=O): 1300–1200 cm^{-1}) (Fig. 3a). Vibrations of ITC are not visible as they are less characteristic and superimposed by other vibrations. Thermogravimetry (TG) is used to determine the total-organics content and indicates a more-or-less continuous thermal decomposition of the nanocarriers up to a temperature of 700 °C (Fig. 3b). After drying in vacuum to remove all surface-adsorbed water and solvents, a mass loss of 74.1 wt% is observed. A solid remain of 25.9 wt% occurred and was identified by XRD as Gd_3PO_7 (Fig. 3c). Furthermore, EA results in a content of 54.3% C, 7.1% H, 3.9% N, and 1.4% S. Hereof, the sulfur content can be assigned to ds as the sole S-containing compound. The N content stems from the drugs ITC and FLP. Considering these data, the as-prepared nanocarriers can be estimated to contain 3.0% ITC, 49.1% Toc, 11.6% ds, 18.7% FLP and 17.6% Gd, resulting in calculated values of 54% C, 7% H, 4% N, 2% S, a total weight loss of 76% and a solid residue of 24%. These calculated values are in good agreement with the experimental data (TG, EA) and also in agreement with the drug load obtained by photometry (see below).

Even more important than the sum composition is the ITC and FLP content of the ITC/Toc@$Gd_2(FLP)_3$ nanocarriers, which was quantified by photometry (Fig. 4). To this concern, the characteristic absorption of ITC at 360 nm and of FLP at 260 nm were measured and compared to reference solutions with known concentration of ITC or FLP (Fig. 4a). For this purpose, calibration curves of both ITC dissolved in ds-stabilized ITC/Toc microemulsions and FLP dissolved in water were recorded (Fig. 4b). The calibration curves show an almost ideal linear dependence between the absorbance of ITC/FLP and the respective concentration in a range of 0–60 µg mL^{-1} (Fig. 4b). Based on the photometrical quantification, the as-prepared suspensions can be concluded to contain ITC/Toc@$Gd_2(FLP)_3$ nanocarriers with a concentration of c(ITC) = 49 µg mL^{-1} and c(FLP) = 317 µg mL^{-1} at a nanocarrier concentration of 1.5 mg mL^{-1}. Here, it needs to be noticed that the superposition of the absorbance at 260 nm was tackled by subtracting the absorbance of ITC from the peak intensity at 260 nm to obtain the absorbance related to FLP. Furthermore, the as-prepared suspensions were diluted by a factor of 12 to guarantee a linear correlation of absorbance and concentration according to the Lambert–Beer law.[16] The ratio of ITC and FLP of 1 : 6.5 determined *via* photometry is also in agreement with the estimation based on the TG and EA results.

Size and structure of ITC/Toc@Gd_2FLP_3 nanocarriers

Size, size distribution, and structure of the as-prepared ITC/Toc@$Gd_2(FLP)_3$ nanocontainers were examined by dynamic light scattering (DLS) and electron microscopy. To this concern, DLS performed with aqueous suspensions lead to a mean hydrodynamic diameter of 63 ± 33 nm (Fig. 5d). A statistical evaluation of >250 nanoparticles on scanning electron microscopy (SEM) images resulted in a slightly smaller diameter of 45 ± 16 nm (Fig. 5a and d), which is in accordance with the larger hydrodynamic diameter stemming from DLS. Scanning transmission electron microscopy (STEM) images confirm the spherical shape and point to the presence of a core@shell structure (Fig. 5b and c). Based on STEM images with higher-resolution, furthermore, the inner cavity diameter as well as the wall thickness can be determined to 40 ± 17 nm and 3–8 nm, respectively.

The core@shell-type structure and the chemical composition are further validated by energy-dispersive X-ray spectroscopy (EDXS). Thus, EDXS element mappings display a uniform distribution of gadolinium, phosphorous, and sulphur around an inner cavity (Fig. 6a–d). These elements reflect the presence of $Gd_2(FLP)_3$ as the nanocarrier shell. Furthermore, EDXS line scans along the orange line on HAADF-STEM images elucidate the core@shell structure with a characteristic dip of the elements Gd, P and S in the center of the nanocarrier (Fig. 6e and f). Here, it must be noticed that the ITC/Toc@$Gd_2(FLP)_3$

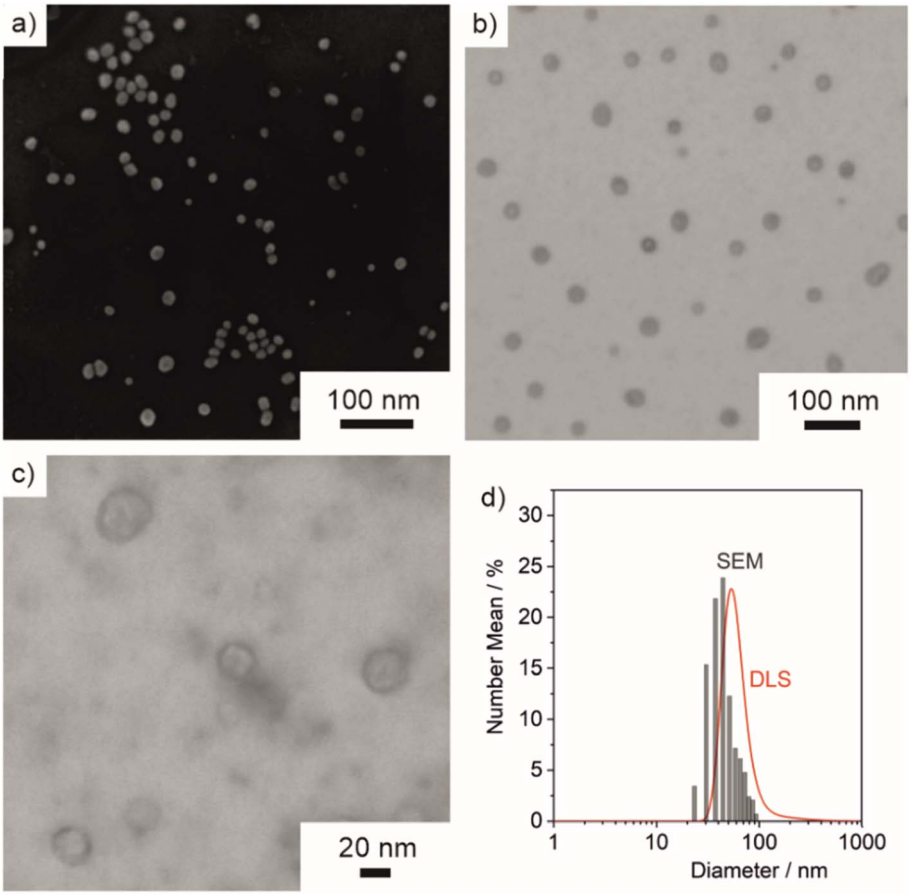

Fig. 5 Size, size distribution, and structure of ITC/Toc@$Gd_2(FLP)_3$ core@shell nanocarriers: (a) SEM image, (b and c) STEM images at different levels of magnification, (d) size distribution according to DLS (in water) and according to statistical evaluation of SEM images (>250 particles).

core@shell nanocarriers show rapid decomposition under the electron beam. This is due to the high organic content and the low conductivity of the nanocarriers as well as due to the bombardment with high-energy electrons causing local heating and charging. Due to the low stability, we have specifically selected larger ITC/Toc@$Gd_2(FLP)_3$ core@shell nanocarriers for EDXS area- and line-scans.

Cytostatic activity of ITC/Toc@$Gd_2(FLP)_3$ nanocarriers

PDAC exhibits a specifically high probability for mutations, which results in a high genetic diversity of the respective cells. Due to the influence of different drugs on the susceptibility of the cells, these mutations can significantly complicate an effective therapy. For this reason, the efficacy of the ITC/Toc@$Gd_2(FLP)_3$ nanocarriers was tested in murine KPC and Panc02 cell lines. Panc02 is a well-established grade III adenocarcinoma model developed by chemical induction with 3-MCA (3-methylcholanthrene) in male C57BL/6 mice,[17] With a mutation of the SMAD4 gene only, Panc02 cells are less relevant in regard of the mutational spectrum of clinically occurring PDAC, nevertheless they are important for preclinical studies to examine nanocarrier uptake and efficacy. Furthermore, KPC cells derived from a KPC mouse representing a transgenic model of PDAC were applied, which exhibit mutations of the KRAS and p53 genes, resulting in non-functional proteins. Therefore, the KPC cell line closely mimmicks the clinical situation, reflecting mutations often occurring for PDAC patients.

To evaluate the efficacy of the as-prepared ITC/Toc@$Gd_2(FLP)_3$ nanocarriers, first of all, an effective uptake of the nanocarriers by tumour cells is essential. For this reason, the uptake of the nanocarriers was assessed by confocal microscopy with cancer cells with different origin (Fig. 7). To prevent premature death of the investigated cells, uptake studies were conducted with drug-free Toc@$Gd_2(AMP)_3$ nanoparticles. These reference nanoparticles (negative control) only contain Toc in the particle core (but no ITC) and $Gd_2(AMP)_3$ with adenosine monophosphate (AMP) as the particle shell. AMP is chemically similar to FLP but does not contain any fluorine at the uridine unit so that DNA reproduction is not blocked. Similar to ITC/Toc@$Gd_2(FLP)_3$, the Toc@$Gd_2(AMP)_3$ reference nanoparticles can be labelled either with DUT 549 or ATTO 647 as a fluorescent dye (Fig. 2).

To account for the genetic versatility of PDAC, the two mouse pancreatic cancer cell lines Panc02 and KPC, the human pancreatic cancer cell line Capan-1 as well as the MH-S macrophage cell line (positive control: murine alveolar macrophages known for efficient uptake of nanoparticles) were

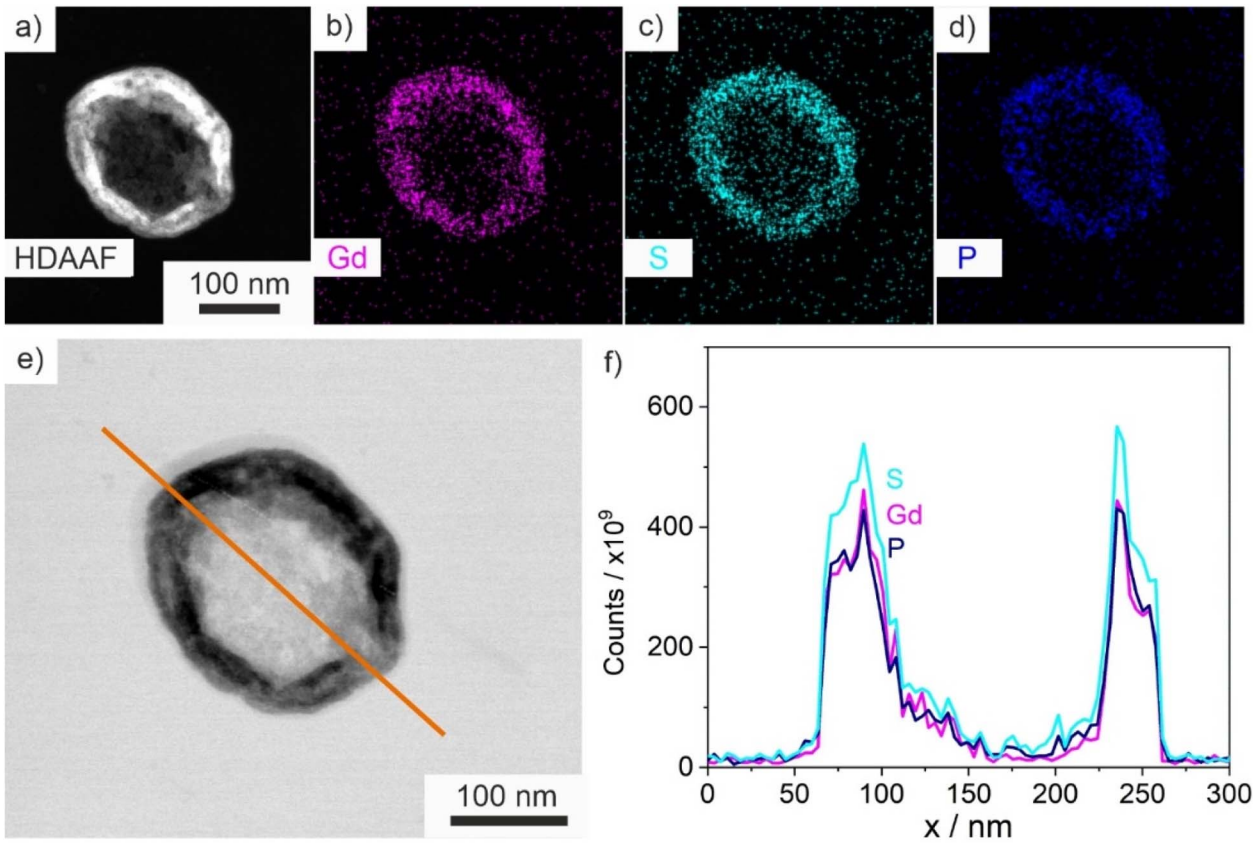

Fig. 6 EDXS of ITC/Toc@$Gd_2(FLP)_3$ nanocarriers: (a) HDAAF-STEM image; (b–d) EDXS element mapping for the nanocarriers on (a) with Gd (b), S (c), and P (d); (e) HDAAF-STEM image with EDXS line scan (f) along the orange line for Gd, S, and P.

treated with Toc@$Gd_2(AMP)_3$ nanoparticles (12.5 ng mL^{-1}). The cell uptake was analysed *via* confocal microscopy 0.5, 5, 24 and 48 h after incubation. ATTO647-labelled Toc@$Gd_2(AMP)_3$ can be clearly detected due to their intense red emission (Fig. 7a–d). Cell nuclei were stained with 4′,6-diamidino-2-phenylindole (DAPI) showing blue emission. A time-dependent uptake of these nanocarriers is clearly visible and indicates a massive nanocarrier concentration not only in the MH-S macrophages (Fig. 7a) but also in all pancreatic cancer cells 48 h after incubation. Due to their high phagocytizing ability, nanocarrier accumulation in MH-S cells was already observed after 5 h. After 24 and 48 h, massive nanocarrier uptake is also observed in all PDAC cells (Fig. 7b–d). Among the PDAC cells, in particular, KPC cells show fast nanocarrier uptake with substantial amounts already observed after 5 h (Fig. 7c).

In addition to PDAC cells, the uptake of the ITC/Toc@$Gd_2(FLP)_3$ nanocarriers was also investigated on other tumour-cell lines to demonstrate their versatility also on a more general level. For this purpose, human skin melanoma cells (SK-Mel-28) and cervical cancer cells (HeLa) were selected and treated with the nanocarriers as well (Fig. 7e and f). Cell uptake was again investigated *via* confocal microscopy 72 h after incubation with suspensions of ATTO 647-labeled ITC/Toc@$Gd_2(FLP)_3$ nanocarriers (50 μg mL^{-1}). With 50 μg mL^{-1} of the nanocarriers, here, a higher concentration was necessary as compared to the treatment of the pancreatic tumour cells (12.5 ng mL^{-1}). Thereafter, the nanocarriers could be clearly visualized in SK-Mel-28 and HeLa cells based on their red fluorescence. The lower nanocarrier uptake in SK-Mel-28 and HeLa cells in comparison to Panc02, KPC, and Capan-1 cells, in fact, could give rise to a possible specificity to tumour cells with high phagocytic activity.

In all tested cells, the nanocarriers predominately accumulate in the perinuclear region (Fig. 7), especially at later time points, suggesting their presence in late endosomal/lysosomal vesicles. We have observed similar intracellular localization patterns also for other, comparable types of nanocarriers, suggesting an endocytic internalization pathway with late endosomal/lysosomal localization after 24 and 48 h, respectively.[25]

The ability of the ITC/Toc@$Gd_2(FLP)_3$ nanocarriers, loaded with the antitumour drugs ITC and FLP, to inhibit cell growth and proliferation of tumour cells was assessed by various *in vitro* studies. For an initial assessment of the cytotoxic activity, ITC/Toc@$Gd_2(FLP)_3$ nanocarriers were examined by MTT toxicity assays, using SK-Mel-28 and HeLa cells as standard cell types (Fig. 8). Herein, the viability of the respective cells was quantified by their ability to reduce the tetrazolium compound 3-(4,5-dimethylthiazol-2-yl)2,5-diphenyltetrazolium bromide (MTT) to formazan. After 72 h of incubation, a clear concentration-dependent effect (5–200 μg mL^{-1}) is visible. ITC/Toc@$Gd_2(FLP)_3$ nanocarriers (red columns) lead to a strong decrease in

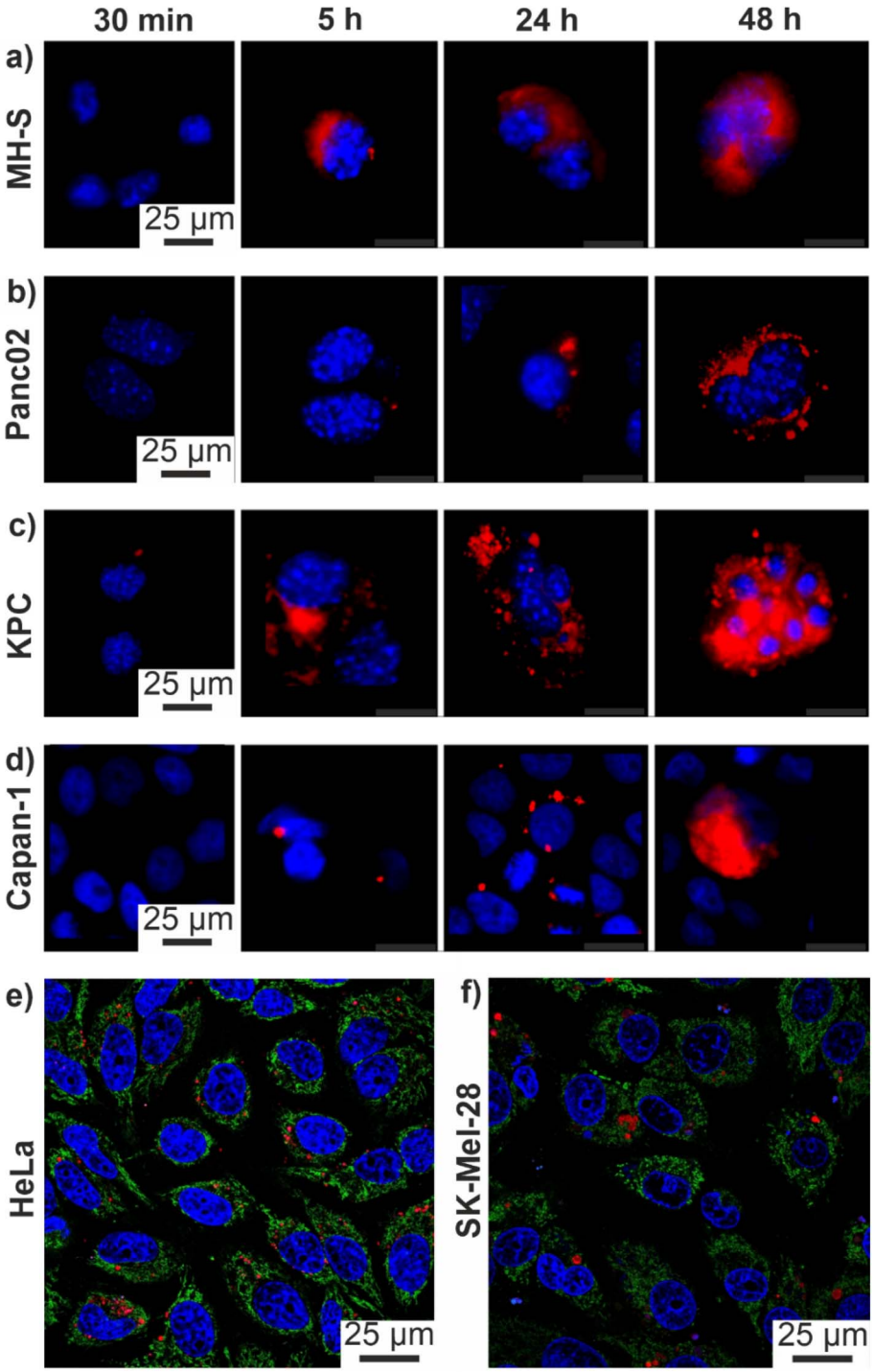

Fig. 7 Cell uptake of core@shell nanocarriers monitored by their red fluorescence: (a–d) confocal microscopy images of ATTO 647-labeled Toc@$Gd_2(AMP)_3$ nanocarriers after uptake (30 min to 48 h) in (a) MH-S, (b) Panc02, (c) KPC, (d) Capan-1 pancreatic cancer cells (red: nanocarriers; blue: DAPI-stained nuclei); (e and f) confocal microscopy images of ATTO 647-labeled ITC/Toc@$Gd_2(FLP)_3$ nanocarriers after 72 h in (e) HeLa cells, (f) SK-Mel-28 cells (red: nanocarriers; blue Hoechst 33342-stained nuclei; green: Mitotracker-stained mitochondria).

cell viability with half-maximal inhibitory concentrations (IC_{50}) of 75 µg mL^{-1} for SKMel28 (Fig. 8b) and 195 µg mL^{-1} for HeLa cells (Fig. 8a), whereas drug-free Toc@$Gd_2(AMP)_3$ nanocarriers (blue columns) as a negative control do not show any considerable effect. The latter points to the absence of non-specific toxic effects of the nanocarriers as such and their non-drug ingredients (*i.e.*, Gd, Toc, ds).

For *in vitro* evaluation of the nanocarrier efficacy, the Panc02 and KPC cells were plated out with a concentration of 15 000 cells per cm^2 and treated with different concentrations of the

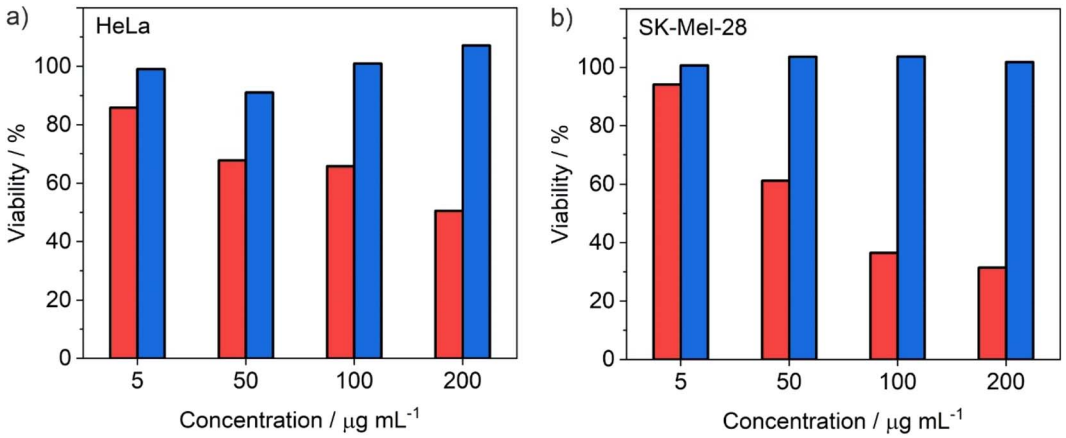

Fig. 8 MTT assays with ITC/Toc@$Gd_2(FLP)_3$ nanocarriers (red columns) and drug-free Toc@$Gd_2(AMP)_3$ nanocarriers as negative control (blue columns) with (a) HeLa cells and (b) SK-Mel-28 cells after 72 h of treatment.

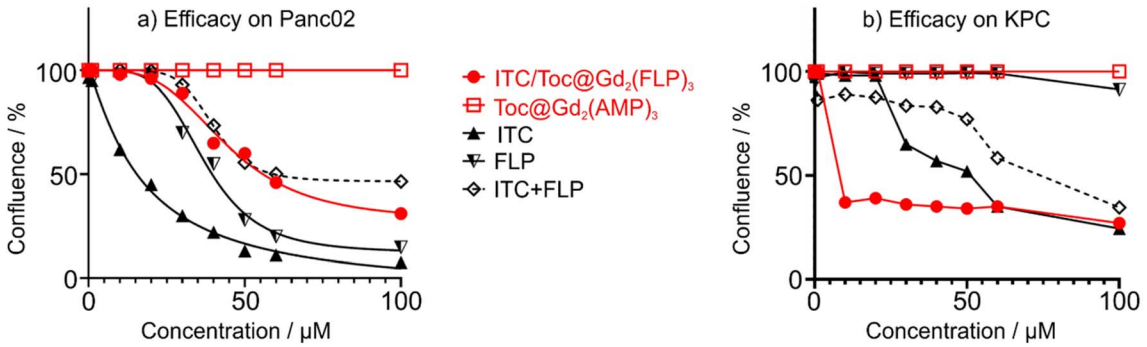

Fig. 9 Cell viability assay of (a) Panc02 and (b) KPC cells *via* live-cell imaging measuring the 72 h response of gradient concentrations (10–100 μM) of ITC/Toc@$Gd_2(FLP)_3$ nanocarriers with free ITC, free FLP, and the combination of both free drugs (ITC + FLP) as positive controls as well as drug-free Toc@$Gd_2(AMP)_3$ nanoparticles as negative control.

ITC/Toc@$Gd_2(FLP)_3$ nanocarriers. Their confluence was measured *via* life-cell imaging once every hour (Fig. 9). The concentration-dependent efficacy was calculated after 72 h of incubation – a point in time when control cells reached 100% confluence. At concentrations ≥ 40 μM (Panc02) and ≥10 μM (KPC), the nanocarriers show high effectiveness in killing both cell types, leading to a significant reduction in confluence. Studies on Panc02 cells show a confluence decrease to 29% (Fig. 9a). In the case of KPC cells, confluence was even further decreased to only 24% (Fig. 9b). Whereas the efficacy of ITC/Toc@$Gd_2(FLP)_3$ nanocarriers on Panc02 cells is already higher compared to the combined free drugs ITC and FLP (as indicated by IC_{50}, *i.e.* the concentration necessary to reduce cell confluence by 50%, Table 1), the most promising efficacy of ITC/Toc@$Gd_2(FLP)_3$ nanocarriers is on KPC cells as further evidenced by their IC_{50} (Table 1). For KPC cells, an IC_{50} of 4.2 μM was calculated after 72 h, which is >10 times lower than for the free drugs ITC (47.7 μM) and FLP (143 μM). This clearly implies the KPC cells to be more sensitive to the ITC/Toc@$Gd_2(FLP)_3$ nanocarrier formulation than to the corresponding free drugs. This also points to the synergistic effect of the ITC/FLP drug cocktail combined in a single type of nanocarriers. While these *in vitro* data already show the efficient uptake, the high efficacy as well as certain selectivity for specific tumor cells, the full potential of the ITC/Toc@$Gd_2(FLP)_3$ nanocarriers can only be unlocked from *in vivo* studies, which also consider selective nanocarrier delivery and potential side effects.

Table 1 Mean inhibitory concentration (IC_{50}, μM) for the treatment of Panc02 and KPC cells with ITC/Toc@$Gd_2(FLP)_3$ nanocarriers and control drugs for the time point of 72 h

Treatment	Panc02 cells	KPC cells
ITC/Toc@$Gd_2(FLP)_3$	46.4	4.2
Free ITC	13.5	47.7
Free FLP	34.2	143.2
Free ITC + FLP	59.4	84.0

Conclusions

After single-drug chemotherapeutic nanocarriers having reached clinical approval, nanocarriers containing a cocktail of chemotherapeutics are the next step for nanocarrier-based tumour treatment. Such adjunctive approach can become most relevant for combinational therapy, particularly in treating

with grim prognosis such as the pancreatic ductal adenocarcinoma (PDAC). This approach allows to simultaneously release high concentrations of drug cocktails at the tumor site, to enhance anticancer efficacy through synergistic or additive effects, to reduce side effects, and/or to minimize the risk of multi-drug resistance. In this regard, we present ITC/Toc@$Gd_2(FLP)_3$ core@shell nanocarriers with a chemotherapeutic cocktail of lipophilic irinotecan (ITC) and hydrophilic fludarabine phosphate (FLP) for the first time.

ITC/Toc@$Gd_2(FLP)_3$ core@shell nanocarriers contain the lipophilic ITC (49 μg mL^{-1}) as the particle core and the hydrophilic FLP (317 μg mL^{-1}) in the particle shell. Size and structure of the nanocarriers are validated by different methods (XRD, FT-IR, TG, EA, photometry, SEM, STEM, HAADF-TEM, EDXS) and result in a total diameter of 45 ± 16 nm, an inner core diameter of 40 ± 17 nm, and a shell thickness of 3–8 nm. With a nanocarrier concentration of 1.5 mg mL^{-1}, aqueous suspensions are colloidally stable over several weeks. For fluorescence detection *in vitro*, the nanocarriers are labelled with Dyomics DUT549P1-aadUTP or ATTO647N-aadUTP to result in green or red emission. The anti-tumour efficacy of ITC/Toc@$Gd_2(FLP)_3$ nanocarriers were studied *in vitro* with mouse and human pancreatic cancer cell lines (Panc02, KPC, Capan-1) and non-PDAC tumour cell lines (SK-Mel-28, HeLa). Specifically for the murine pancreatic KPC cancer cells, ITC/Toc@$Gd_2(FLP)_3$ nanocarriers show very promising efficacy with an inhibitory concentration (IC_{50}: 4.2 μM) outperforming the free drugs (ITC: 47.7 μM, FLP: 143 μM) more than 10 times. This aligns with the impressively early uptake of the high amounts of the IOH-NPs by KPC cells as observed by fluorescence microscopy.

With these results, the core@shell chemotherapeutic cocktail concept can become a highly promising tool for future drug delivery strategies and combined chemotherapies especially for the treatment of pancreatic cancer with poor prognosis. Following the establishment of the synthesis strategy of core@shell dual-drug nanocarriers, an adjustment of drug content and drug synergistic ratio as well as a transfer to other drugs are intended and offer additional options for synthesis and material concepts.

Conflicts of interest

The authors declare no competing financial interests.

Acknowledgements

D. R., J. P., U. S. and C. F. thank the Deutsche Forschungsgemeinschaft (DFG) for funding within the Research Training Group 2039. Moreover, J. N. and C. F. are grateful to the DFG for funding with in the project "Synergistic Image-guided Nanoparticles for Drug Delivery (SIN-Drug)". J. P. also thanks the Ministerium für Ernährung, Ländlichen Raum und Verbraucherschutz Baden-Württemberg (MLR) for financial support. U. S. thanks for funding under the Germany's Excellence Strategy *via* the Excellence Cluster "3D Matter Made to Order (EXC-2082/1-390761711)". The work of J. P. and U. S. was also supported by the Helmholtz Program Materials Systems Engineering (MSE). Finally, the authors acknowledge Jacqueline Stier and Bärbel Heidrich for excellent assistance in experiments.

References

1 (*a*) F. Farjadian, A. Ghasemi, O. Gohari, A. Roointan, M. Karimi and M. R. Hamblin, *Nanomedicine*, 2019, **14**, 93–126; (*b*) D. Peer, J. M. Karp, S. Hong, O. C. Farokhzad, R. Margalit and R. Langer, *Nat. Nanotechnol.*, 2007, **2**, 751–760.

2 (*a*) Y. Barenholz, *J. Controlled Release*, 2012, **160**, 117–134; (*b*) W. J. Gradishar, S. Tjulandin, N. Davidson, H. Shaw, D. Heather, N. Desai, P. Bhar, M. Hawkins and J. O'Shaughnessy, *J. Clin. Oncol.*, 2005, **23**, 7794–7803.

3 (*a*) S. Kunjachan, J. Ehling, G. Storm, F. Kiessling and T. Lammers, *Chem. Rev.*, 2015, **115**, 10907–10937; (*b*) T. L. Doane and C. Burda, *Chem. Soc. Rev.*, 2012, **41**, 2885–2911.

4 (*a*) P. H. D. Nguyen, M. K. Jayasinghe, A. H. Le, B. Peng and M. T. N. Le, *ACS Nano*, 2023, **17**, 5187–5210; (*b*) K. Ulbrich, K. Hola, V. Subr, A. Bakandritsos, J. Tucek and R. Zboril, *Chem. Rev.*, 2016, **116**, 5338–5431.

5 (*a*) T. Senthilkumar, L. Zhou, Q. Gu, L. Liu, F. Lv and S. Wang, *Angew. Chem., Int. Ed.*, 2018, **57**, 13114–13119; (*b*) C. D. Spicer, C. Jumeaux, B. Gupta and M. M. Stevens, *Chem. Soc. Rev.*, 2018, **47**, 3574–3620; (*c*) K. Ulbrich, K. Hola, V. Subr, A. Bakandritsos, J. Tucek and R. Zboril, *Chem. Rev.*, 2016, **116**, 5338–5431.

6 (*a*) T. M. Allen and P. R. Cullis, *Adv. Drug Deliv. Rev.*, 2013, **65**, 36–48; (*b*) S. Parveen, R. Misra and S. K. Sahoo, *Nanomedicine*, 2012, **8**, 147–166.

7 (*a*) A. Jozefczak, K. Kaczmarek and R. Bielas, *Theranostics*, 2021, **11**, 10091–10113; (*b*) M. Manzano and M. Vallet-Regi, *Adv. Funct. Mater.*, 2020, **30**, 1902634; (*c*) S. Zhao, X. Yu, Y. Qian, W. Chen and J. Shen, *Theranostics*, 2020, **10**, 6278–6309.

8 T. Conroy, C. Gavoille, E. Samalin, M. Ychou and M. Ducreux, *Curr. Oncol. Rep.*, 2013, **15**, 182–189.

9 A. Detappe, H. V. T. Nguyen, Y. Jiang, M. P. Agius, W. Wang, C. Mathieu, N. K. Su, S. L. Kristufek, D. J. Lundberg, S. Bhagchandani, I. M. Ghobrial, P. P. Ghoroghchian and J. A. Johnson, *Nat. Nanotechnol.*, 2023, **18**, 184–192.

10 (*a*) D. Rudolph, N. Redinger, K. Schwarz, F. Li, G. Hädrich, M. Cohrs, L. A. Dailey, U. E. Schaible and C. Feldmann, *ACS Nano*, 2023, **17**, 9478–9486; (*b*) M. Khorenko, A. Meschkov, J. Napp, J. Pfeifer, J. Stier, F. Alves, U. Schepers and C. Feldmann, *J. Mater. Chem. B*, 2023, **11**, 3635–3649; (*c*) V. Rein, E. Zittel, K. Hagens, N. Redinger, U. Schepers, H. Mehlhorn, U. Schaible and C. Feldmann, *Adv. Funct. Mater.*, 2019, **29**, 1900543.

11 W. Hiddemann, R. Rottmann, B. Wörmann, A. Thiel, M. Essink, C. Ottensmeier, M. Freund, T. Büchner and J. van de Loo, *Ann. Hematol.*, 1991, **63**, 1–4.

12 R. H. J. Mathijssen, R. J. van Alphen, J. Verweij, W. J. Loos, K. Nooter, G. Stoter and A. Sparreboom, *Clin. Cancer Res.*, 2001, **7**, 2182–2194.

13 S. Stevanović, L. M. Draper, M. M. Langhan, T. E. Campbell, M. L. Kwong, J. R. Wunderlich, M. E. Dudley, J. C. Yang, R. M. Sherry, U. S. Kammula, N. P. Restifo, S. A. Rosenberg and C. S. Hinrichs, *J. Clin. Oncol.*, 2015, **33**, 1543–1550.
14 (*a*) M. Orth, P. Metzger, S. Gerum, J. Mayerle, G. Schneider, C. Belka, M. Schnurr and K. Lauber, *Radiat. Oncol.*, 2019, **14**, 141–161; (*b*) T. Y. S. Le Large, M. F. Bijlsma, G. Kazemier, H. W. M. van Laarhoven, E. Giovannetti and C. R. Jimenez, *Semin. Cancer Biol.*, 2017, **44**, 153–169.
15 E. S. Christenson, E. Jaffee and N. S. Azad, *Lancet Oncol.*, 2020, **21**, e135.
16 T. G. Mayerhöfer, A. V. Pipa and J. Popp, *ChemPhysChem*, 2019, **20**, 2748–2753.
17 T. H. Corbett, B. J. Roberts, W. R. Leopold, J. C. Peckham, L. J. Wilkoff, D. P. Griswold and F. M. Schabel, *Cancer Res.*, 1984, **44**, 717–726.
18 S. R. Hingorani, L. Wang, A. S. Multani, C. Combs, T. B. Deramaudt, R. H. Hruban, A. K. Rustgi, S. Chang and D. A. Tuveson, *Cancer Cell*, 2005, **7**(5), 469–483.
19 J. W. Lee, C. A. Komar, F. Bengsch, K. Graham and G. L. Beatty, *Curr. Protoc. Pharmacol.*, 2016, **73**, 14.39.1–14.39.20.
20 A. P. Kyriazis, A. A. Kyriazis, D. G. Scarpelli, J. Fogh, M. S. Rao and R. Lepera, *Am. J. Pathol.*, 1982, **106**(2), 250–260.
21 I. N. Mbawuike and H. B. Herscowitz, *J. Leukoc. Biol.*, 1989, **46**, 119–127.
22 W. S. Rasband, *ImageJ*, U. S. National Institutes of Health, Bethesda, Maryland, USA, 1997–2018, **https://imagej.net/ij/**.
23 A. Kamal-Eldin and L. A. Appelqvist, *Lipids*, 1996, **31**, 671–701.
24 R. Jog and D. J. Burgess, *J. Pharmaceut. Sci.*, 2017, **106**, 39–65.
25 M. Ischyropoulou, K. Sabljo, L. Schneider, C. M. Niemeyer, J. Napp, C. Feldmann and F. Alves, *Adv. Mater.*, 2023, 2305151.